MAGNETIC PARTICLE MOTIONS WITHIN LIVING CELLS

Physical Theory and Techniques

P. A. VALBERG AND J. P. BUTLER

Department of Environmental Science and Physiology, Harvard School of Public Health, Boston, Massachusetts 02115

ABSTRACT Body tissues are not ferromagnetic, but ferromagnetic particles can be present as contaminants or as probes in the lungs and in other organs. The magnetic domains of these particles can be aligned by momentary application of an external magnetic field; the magnitude and time course of the resultant remanent field depend on the quantity of magnetic material and the degree of particle motion. The interpretation of magnetometric data requires an understanding of particle magnetization, agglomeration, random motion, and both rotation and translation in response to magnetic fields. We present physical principles relevant to magnetometry and suggest models for intracellular particle motion driven by thermal, elastic, or cellular forces. The design principles of instrumentation for magnetizing intracellular particles and for detecting weak remanent magnetic fields are described. Such magnetic measurements can be used for noninvasive studies of particle clearance from the body or of particle motion within body tissues and cells. Assumptions inherent to this experimental approach and possible sources of artifact are considered and evaluated.

INTRODUCTION

The presence of minute quantities of ferromagnetic (or ferrimagnetic) material within human subjects was first detected by Cohen (1973) while monitoring physiological magnetic fields from cardiac electric currents. Cohen realized that the field observed after magnetization (the remanent field) could be used to determine the quantity of contaminating particles in the body. The lung content of magnetic material has been measured by this means in workers occupationally exposed to airborne dusts (Cohen, 1975; Freedman et al., 1980; Kalliomäki et al., 1980). The principles behind magnetic evaluation of lung retention have been discussed (Cohen and Nemoto, 1984; Cohen et al., 1984). Cohen (1973) also noted that, unexpectedly, the remanent field from the lungs decreased by as much as a factor of six during the first hour after magnetization. Since the particle magnetization is permanent, this remanent-field decay could only be the result of random particle rotation away from the original direction of magnetization. Cohen called this process "relaxation" and attributed it to an unidentified viable process driving the motion of lung-retained particles.

Possible mechanisms for relaxation of magnetic particles within lungs include lung ventilatory movements, cardiovascular pulsations, ciliary beating, surfactant and mucus flow, gastrointestinal peristalsis, Brownian motion, and cytoplasmic motions in cells containing particles. The last mechanism stems from the fact that lung surfaces are populated by motile cells, lung macrophages, that recognize foreign particles and ingest them into membrane-bound vesicles called phagosomes (Sorokin and Brain, 1975). Relaxation was also observed in hamsters after intravenous injection of magnetite (Gehr et al., 1983*a*). Macrophages lining blood sinusoids in the liver took up the magnetic material, and particle reorientation in this case could only be driven by blood flow, cytoplasmic motion, and Brownian motion. For intact animals, interpretation of the relaxation phenomenon is problematic. A variety of mechanisms may contribute to relaxation, and particles can be found at different anatomical sites (e.g., alveolar surface, lymph nodes, interstitium, airways, gut). These problems were avoided by measuring relaxation for macrophages in culture, where complications of tissue movements, many anatomical compartments, heterogeneous cell types, variable geometry, and noncellular magnetic contamination are not present. Animals first inhaled airborne magnetic particles (γ-Fe_2O_3). Pulmonary macrophages were collected one day later by lung lavage and examined using both magnetometry and time-lapse videomicroscopy. The relaxation phenomenon was demonstrated to be associated with macrophage cytoplasmic motions, which reoriented the alignment of intracellular magnetic iron oxide particles (Valberg, 1984; Valberg and

Address correspondence to Peter A. Valberg, Department of Environmental Science and Physiology, Harvard School of Public Health, 665 Huntington Avenue, Boston, MA 02115.

Albertini, 1985). Now the emphasis has turned to the use of intracellular particles as non-optical probes of the motions and physical properties of cytoplasm.

The nature of, guidance of, and regulation of intracellular vesicle movements are all poorly understood. Cell organelles containing ferromagnetic material give rise to magnetic field signals that can provide information about the physical movements within living cells. In this paper we present physical principles, mechanistic models, and instrumental techniques involved in cell magnetometry. The following paper discusses cell preparation, statistical analysis of magnetometric signals, and results for normal cells, for cytochalasin-D–treated cells, and for different magnetization protocols (Valberg and Feldman, 1987).

PARTICLE RESPONSE TO MAGNETIC FIELDS

Ferromagnetic Materials

Body tissues are either weakly paramagnetic or weakly diamagnetic. That is, body constituents (including iron-containing proteins) do not exhibit residual magnetization after application and removal of external magnetic fields. In contrast, ferromagnetic particles contain regions of spontaneous magnetization, called magnetic domains, even in the absence of applied fields. A consequence of this difference in magnetic behavior is that the presence in body tissues of small quantities of ferromagnetic contaminants can be detected and their magnetic orientation monitored. Ferromagnetic behavior is not a property of individual molecules but is due to a cooperative interaction between many molecules in bulk material. For example, ferromagnetic material loses its magnetic properties when it dissolves.

Not every ferromagnetic particle or collection of particles is a strong magnet because many different directions of magnetization may be represented by randomly oriented magnetic domains within a single particle or among separate particles. Ferromagnetic material can become permanently magnetized through application of a strong magnetic field, $\geq$50 mT, which causes favorably oriented domains to grow in size and other domains to rotate into alignment with the applied field lines. Domain walls adjust rapidly, moving at a speed of $\sim$35 μm/μs for magnetic iron oxides. The domain boundary movements produced by magnetization remain after removal of the external field, and the material generates a substantial remanent magnetic field. The remanent magnetization will maintain its magnitude and direction even in the presence of changing environmental fields as long as the coercive field strength, H_c, is not exceeded. The coercivity of "hard" ferromagnetic materials (such as γ-Fe_2O_3) varies from 5 to 250 mT and is indicative of the force required for magnetic domain reorientation.

The specific properties of particulate magnetic iron oxides have been studied in detail because of their importance in magnetic recording. Data on acicular γ-Fe_2O_3 from a recent review (Bate, 1980) are summarized in Table I (SI units will be used throughout). Some particle properties, notably ρ, M_s (saturation magnetic moment per unit volume) and σ_s (saturation magnetic moment per unit weight), are size independent, whereas M_r (remanent magnetic moment per unit volume), σ_r, and H_c can show size and shape effects. For example, material in the form of a circumferentially magnetized ring can have remanent magnetization equal to saturation magnetization, $\sigma_r/\sigma_s = 1$. However, for a random array of monodomain uniaxial particles, $\sigma_r/\sigma_s \approx 0.5$. The remanent field produced after magnetization of a particle or sample depends on the geometry of the sample. The demagnetizing factor, N_d, expresses how the field produced by a particle acts to demagnetize the particle. The demagnetizing field, H_d, acts in the opposite direction, but is proportional to, the magnetization M which creates it:

$$\mathbf{H}_d = -\frac{N_d}{\mu_o}\mathbf{M} \qquad (\mu_o = 4\pi \times 10^{-7}\mathrm{N/A^2}). \tag{1}$$

N_d depends on particle shape: For a prolate (cigar-shaped) ellipsoid magnetized parallel to its length with length-diameter ratio 10:1, where $N_d \approx 0.02$, particle magnetization is barely affected. For an oblate (pancake-shaped) ellipsoid magnetized parallel to its short axis with length-diameter ratio 1:10, where $N_d \approx 0.90$, demagnetization is significant. For a sphere, $N_d \approx 0.33$. The net effect is that when N_d is large, the material resists magnetization, and the remanent field produced is small. It is important to consider these shape effects when assuming remanent field

TABLE I

Gamma iron oxide particle properties	
Density ρ	4,600 kg/m^3
Particle length range	0.05–0.7 μm
Axial ratio	3:1–10:1
Monodomain behavior range	0.03–1.5 μm
Saturation magnetization, σ_s	78 A-m^2/kg
Remanent magnetization, σ_r	36.2 A-m^2/kg
Coercive field, H_c	16–36 kA/m (20–45 mT)
Anisotropy energy	$\frac{2}{3}$ shape, $\frac{1}{3}$ crystal
Representative particle	
Volume equivalent diameter sphere	0.43 μm
Axial lengths (prolate)	a = 0.9 μm, b = 0.3 μm
Axial ratio	3:1
Volume	0.042 μm^3
Mass	0.20 $\mu\mu$g
Magnetic moment, **m**	1.6 $\times$ 10^{-14} A-m^2
Coercive field, H_c	20 kA/m (25 mT)
Geometric factors (see Eqs. 9 and 13)	
ϵ	0.943
ζ	1.95
κ	17.5
$N_a - N_b$ (multidomain)	0.34

In free space: 1 mT = 796 A/m = 10 gauss = 10 oersted.

magnitude is proportional to the amount of magnetic material present.

Coercivity, or resistance to changes in magnetization, also varies with particle shape and size; the coercive field of elongated particles can be 10^4 times that of bulk material. In general, H_c varies inversely with particle diameter for both single domain and multidomain particles. However, below ~2-nm diam, particle magnetization becomes unstable and changes direction spontaneously due to thermal energy; coercivity rapidly drops to zero.

Twisting Particles with an External Magnetic Field

Ferromagnetic particles dispersed in a fluid medium will respond to a uniform magnetic field much like compass needles, that is, by rotating into magnetic alignment at a rate that depends upon the viscosity of the fluid suspension. Therefore, the particle rotation rate can be used to measure the viscosity of the surrounding fluid. An ellipsoidal particle rotating at an angular velocity ω in a Newtonian fluid of viscosity η will experience a hydrodynamic retarding torque ($\mathbf{N}_{hyd}$) given by

$$\mathbf{N}_{hyd} = -\kappa V \eta \omega, \tag{2}$$

where V is the volume of the particle, and κ is the particle shape factor.

The magnetic torque ($\mathbf{N}_{mag}$) applied by an external field ($\mathbf{H}_a$) on a particle of magnetization per unit volume of $\mathbf{M}$ is

$$\mathbf{N}_{mag} = \int_V \mu_o(\mathbf{M} \times \mathbf{H}_a)dV. \tag{3}$$

This integral is difficult to evaluate in the general case because $\mathbf{M}$ is influenced by $\mathbf{H}_a$, can vary spatially within a particle, and is dependent on particle shape and magnetic properties. However, two simplified situations are illuminating: (*a*) particles of constant remanent magnetization in low fields ($H_a < H_c$) and (*b*) particles in high fields where M and H_a are parallel and $|\mathbf{M}| \approx M_{sat}$.

(*a*) For particles of constant magnetization, the magnetic torque can be expressed in terms of the particle magnetic moment ($\mathbf{m}$):

$$\mathbf{N}_{mag} = \mu_o \mathbf{m} \times \mathbf{H}_a, \qquad \text{where } m = V M_r. \tag{4}$$

The magnitude of the torque depends only on the sine of the angle θ between the directions of $\mathbf{m}$ and $\mathbf{H}_a$. The equation of motion with particle moment of inertia, I, and angular velocity, ω, is

$$\mathbf{N}_{mag} = I\frac{\partial \omega}{\partial t} - \mathbf{N}_{hyd}. \tag{5}$$

Since inertial behavior can be neglected (illustrated in Fig. 1), the two torques are balanced:

$$\mathbf{N}_{mag} = \mathbf{N}_{hyd}. \tag{6}$$

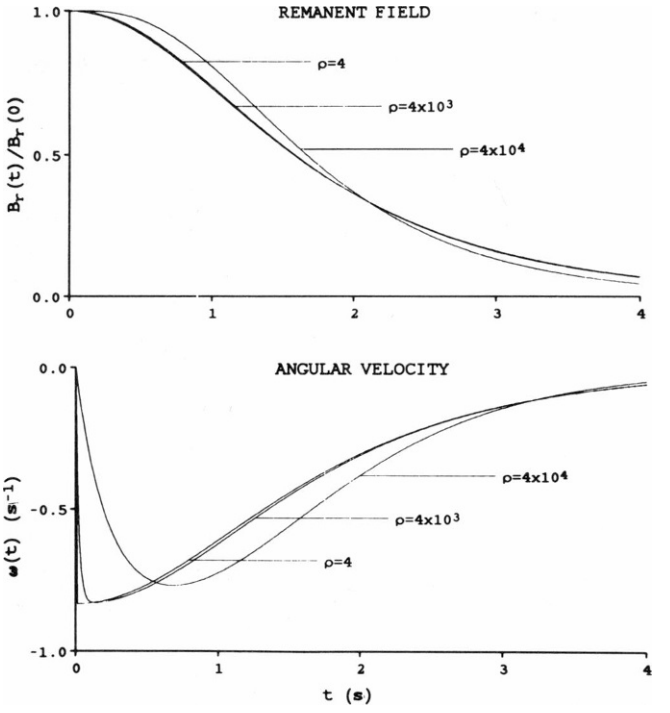

FIGURE 1 *Top*, $B_r(t)/B_{r0}$, *bottom*, $\omega(t)$ in s^{-1}, showing the result of numerical integration of Eq. 5 for magnetic particles rotating in a Newtonian fluid (η = 100 Pa-s). Particles are twisted beginning at $t = 0$ from an initially aligned position where $B_r(t)/B_{r0} = 1.0$. The twisting field (2.5 mT) is perpendicular to the direction of particle magnetic moments at $t = 0$. Three separate values of particle density have been plotted to illustrate that inertia can be ignored. The specific gravity of the particles has to reach 4,000 before significant deviation from inertia-free conditions is seen for the time dependence of the remanent field or the particle angular velocity.

This yields a differential equation expressing how the angle θ between $\mathbf{H}_a$ and the particle's magnetization direction decreases as a function of time:

$$\frac{\partial \theta}{\partial t} = -\frac{mH_a}{\kappa V \eta}\sin\theta. \tag{7}$$

If $\theta = \theta_o$ at $t = 0$, integration gives the result:

$$\tan(\theta/2) = \tan(\theta_o/2)\,(e^{-t/\tau_{lo}}) \qquad \text{where } \tau_{lo} = \left(\frac{\kappa\eta}{\mu_o M_r H_a}\right), \tag{8}$$

where, for ellipsoidal particles of major and minor axes a and b, the following definitions for V and κ apply (Edwardes, 1893):

$$V = \frac{\pi a b^2}{6}$$

$$\kappa = \frac{1.6[3(a/b)^2 + 2]}{1 + \zeta - 0.5\,\zeta(b/a)^2}$$

where

$$\zeta = \frac{1}{\epsilon^3}\left[\ln\left(\frac{1+\epsilon}{1-\epsilon}\right) - 2\epsilon\right]$$

where

$$\epsilon = \sqrt{1 - (b/a)^2} \qquad (a \geq b). \tag{9}$$

For a sphere ($a = b$), $\epsilon = 0$, $\zeta = \frac{2}{3}$, $\kappa = 6$.

If the remanent field, $B_r(t)$, is measured along the original direction (θ_o) of particle magnetic moment, then as the particle is rotated away from this direction by the twisting field, $B_r(t)$ decreases from its initial value (B_{r0}) as

$$B_r(t) = B_{r0} \cos(\theta_o - \theta). \tag{10}$$

In the particular case of $\theta_o = 90°$, Eqs. 8 and 10 can be combined to give

$$B_r(t) = B_{r0} \operatorname{sech}(t/\tau_{lo}) = B_{r0} \operatorname{sech}\left(\frac{\mu_o M_r H_a t}{\kappa\eta}\right). \tag{11}$$

This expression is independent of particle size. Also, the twisting field and time appear as a product ($H_a t$). Comparisons of the twisting effects for magnetic pulses of equivalent $H_a t$ (increasing H_a, decreasing t) can be used to probe non-Newtonian behavior, i.e., the dependence of η on shear rate.

We dispersed the γ-Fe_2O_3 particles used in macrophage experiments in dimethylpolysiloxane fluids (200 Fluids, Dow Corning Corp., Midland, MI) of calibrated viscosity ranging from 60 Pa-s (0.6 kP) to 600 Pa-s (6 kP) ($H_2O \approx$ 0.0007 Pa-s = 0.007 poise). A torque was applied to the magnetized particles with a weak field (2.5 mT) applied perpendicular to the initial particle alignment direction. For particles embedded in epoxy, the remanent field was unchanged, and for the high-viscosity Newtonian fluids, the remanent field decreased at a rate that depended inversely on viscosity (Fig. 2). We compared the data to the above predictions for twisting of constant-magnetization particles. Three conclusions could be drawn. First, the shape of the twisting curve is consistent with the form predicted by Eq. 11 (cf. Fig. 1). Second, the coercivity of the particles is not exceeded by a field of 2.5 mT, since particles embedded in epoxy show no change in magnetization. Third, the numerical value for viscosity predicted by fitting Eq. 11 to the data in Fig. 2 is higher than the known fluid viscosity. This would be expected if the hydrodynamic radius of the particles were ~1.7× larger than the magnetic radius. That is, the particles have voids and fissures that are filled with nonmagnetic, nonmoving fluid; the particle then behaves hydrodynamically as an object of lower magnetic moment than if it were solid magnetic iron oxide. Hence, the data for twisting particles in viscosity standards can be viewed as calibrating the remanent magnetization per unit volume, M_r, for particles that trap nonmagnetic fluid within porosities.

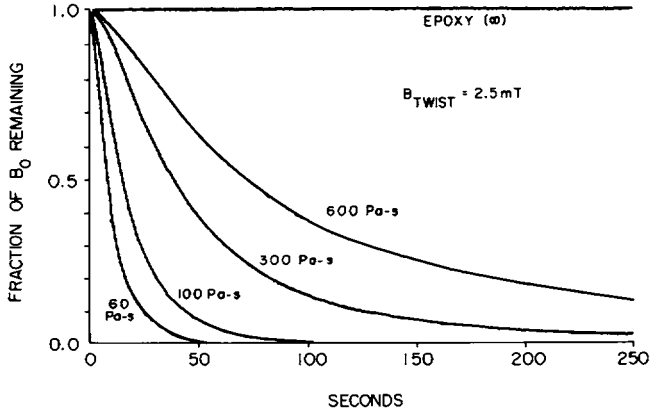

FIGURE 2 The remanent field from particles suspended in viscosity standards. The particles were magnetized and a twisting field was applied at right angles to the initial magnetization. These data were used to estimate the viscous environment of particles within cells.

(*b*) Particles in high fields have M and H_a parallel ($M \approx M_{sat}$), and the torque is due to particle shape anisotropy. The magnetic energy of an elongated (prolate ellipsoid) particle depends on the angle it makes with the field (Brown, 1962):

$$E = \tfrac{1}{2}\mu_o(N_a - N_b)VM_s^2 \sin^2\theta, \tag{12}$$

where θ is the angle between the long axis of the ellipsoid and the applied field, and N_a and N_b are the demagnetizing factors along the long and short axes. In terms of the earlier definition of ζ, these can be expressed as

$$N_a = \tfrac{1}{2}\zeta(b/a)^2 \qquad \text{and} \qquad N_b = 1 - \zeta(b/a)^2. \tag{13}$$

The magnitude of the torque acting to align the long axis of the particle with the field direction can be obtained by differentiating the expression for energy with respect to θ:

$$N_{mag} = \mu_o(N_a - N_b)VM_s^2 \sin\theta\cos\theta. \tag{14}$$

The torque is maximum at 45°, is independent of the size of the applied field (as long as $M \approx M_2$), and is considerably larger here than in the low-field case. The solution for θ in this case is

$$\tan(\theta) = \tan(\theta_o)\, e^{t/\tau_{hi}}, \quad \text{where} \quad \tau_{hi} = \frac{\kappa\eta}{\mu_o(N_a - N_b)M_s^2}. \tag{15}$$

Again, if the remanent field, $B_r(t)$, is measured along the particle's original direction of magnetization, and if θ_o = 45° at $t = 0$, then $B_r(t)$ is related to the initial field, B_{r0}, by

$$B_r(t) = \frac{B_{r0}}{\sqrt{1 + e^{2t/\tau_{hi}}}}. \tag{16}$$

It is useful to calculate the size of the characteristic time constant τ of particle reorientation for a series of three viscosities: water at 37°C, $\eta \sim 0.0007$ Pa-s; glycerol at 25°C, $\eta \sim 1.0$ Pa-s; cell apparent viscosity at 37°C, $\eta \sim$ 1200 Pa-s; and for a series of three applied fields: the earth's field ~0.05 mT, low-field twisting at 2.5 mT, and high-field magnetization at >100 mT. The results are shown in Table II.

TABLE II
CHARACTERISTIC TWIST TIME, τ_{lo} or τ_{hi}

Twist field (H_a)	Fluid viscosity η (Pa-s)		
	0.0007	1.0	1,200
mT			
0.05	3.3 ms	4.8 s	96 min
2.5	67 μs	0.1 s	2 min
>100	1 μs	1.5 ms	0.2 s

Particle-Particle Magnetic Interactions

Magnetized particles exert forces on each other, and it is necessary to take these forces into account. The energy of interaction of the two magnetic dipoles $\mathbf{m}_1$ and $\mathbf{m}_2$, as shown in Fig. 3 is

$$E = \frac{\mu_o}{4\pi} \frac{\mathbf{m}_1 \cdot \mathbf{m}_2 - 3(\mathbf{m}_1 \cdot \hat{\delta})(\mathbf{m}_2 \cdot \hat{\delta})}{|\mathbf{r}|^3}, \tag{17}$$

where $\hat{\delta}$ is the unit vector along the line separating the two dipoles. The magnitude of the radial force acting on dipole 2 due to the presence of dipole 1 is

$$F_r = -(\mu_o/4\pi)(3m_1m_2/r^4)[3\cos\theta_1\cos\theta_2 - \cos(\theta_1 - \theta_2)].$$

The tangential force is

$$F_\theta = -(\mu_o/4\pi)(m_1m_2/r^4)[3\sin\theta_1\cos\theta_2 - \sin(\theta_1 - \theta_2)].$$

The torque on dipole 2 due to the presence of dipole 1 is

$$N_\theta = -(\mu_o/4\pi)(m_1m_2/r^3)[3\cos\theta_1\sin\theta_2 - \sin(\theta_1 - \theta_2)].$$

When the two dipoles are oriented in the same direction along the line joining them (head-to-tail or $\theta_1 = \theta_2 = 0°$) the force is attractive and of magnitude $6\mu_o m_1 m_2/4\pi r^4$. When the dipoles are lined up but oriented at 90° to the line joining them (side-by-side or $\theta_1 = \theta_2 = 90°$) the force is repulsive and of magnitude $3\mu_o m_1 m_2/4\pi r^4$. If dipoles are parallel to each other ($\theta_1 = \theta_2$), but not parallel to the line joining them, the effect of the F_θ force is to drive them into a head-to-tail orientation. At intermediate orientations, there is both a radial and a tangential force that generally acts to drive the dipoles either into parallel head-to-tail configuration or an antiparallel side-by-side configuration.

Magnetic particles dispersed in a fluid may readily agglomerate if the particle concentration is sufficiently high. Magnetic particles suspended in water will orient along the earth's magnetic field in a few milliseconds (Table II), and since the energy of this interaction is ~200 kT, they will maintain this orientation. The time course of particle movement can be calculated for two lined-up dipoles of radius a, with dipole moment m ($m = \frac{4}{3}\pi a^3 M_r$, and separated by a distance z. Inertial effects can be neglected, and viscous forces are balanced by magnetic forces

$$0 = F_{\text{dipole-dipole}} + 6\pi\eta a v \tag{18}$$

$$-\frac{8\mu_o a^6 M_r^2}{3z^4} = 6\pi\eta a v. \tag{19}$$

Setting $v = dz/dt$, and integrating ($z = z_o$ at $t = 0$), we find

$$z = z_o\left[1 - \left(\frac{a}{z_o}\right)^5 \left(\frac{t}{\tau_{dd}}\right)\right]^{1/5},$$

where

$$\tau_{dd} = \frac{9\eta}{20\,\mu_o M_r^2}. \tag{20}$$

Particle separation decreases as shown in Fig. 4. When $z = a$ particle separation becomes zero, which occurs at a time

$$t_{z=a} = \tau_{dd}\left[\left(\frac{z_o}{a}\right)^5 - 1\right] = \tau_{agglom}. \tag{21}$$

Suppose magnetic particles, radius a and density ρ_{part}, are suspended in a fluid at a concentration of $\rho_{wt/vol}$ particle mass per unit fluid volume, then the initial average particle–particle separation is

$$z_o = a\left(\frac{4\pi\rho_{part}}{3\rho_{wt/vol}}\right)^{1/3}, \tag{22}$$

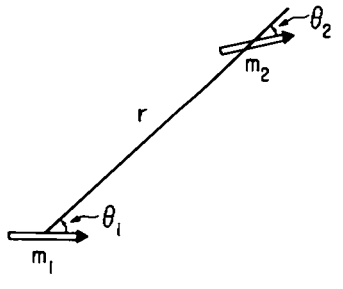

FIGURE 3 Two magnetic dipoles interact to produce forces on each other that depend on their separation, r, and relative orientation, θ_1 and θ_2.

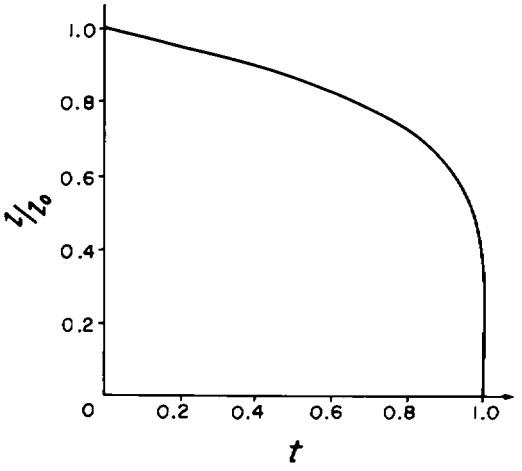

FIGURE 4 Time course of interparticle separation for two dipoles aligned head-to-tail, initially at a separation z_o. Time is plotted as a fraction of τ_{agglom}, Eq. 21.

and assuming $(z_o/a)^5 \gg 1$,

$$\tau_{\text{agglom}} \approx \left(\frac{9\eta}{20\mu_o M_r^2}\right)\left(\frac{4\pi\rho_{\text{part}}}{3\rho_{\text{wt/vol}}}\right)^{5/3}. \quad (23)$$

Upon substituting M_r appropriate to γ-Fe_2O_3 (Table I), we have

$$\tau_{\text{agglom}} \approx (0.1\ \mu\text{s}) \cdot \left(\frac{\eta}{\eta_{H_2O}}\right) \cdot \left(\frac{\rho_{\text{part}}}{\rho_{\text{wt/vol}}}\right)^{5/3}. \quad (24)$$

For example, a water suspension of 2 mg γ-Fe_2O_3 particles per milliliter fluid ($\rho_{\text{wt/vol}}$ = 2 mg/ml; ρ_{part} = 4,600 mg/ml) is typical of solutions used to instill magnetic particles in animals (Brain et al., 1984; Gehr et al., 1983*b*; Nemoto et al., 1985). The above calculations indicate that the particles in the instillate are not individual ones, but will agglomerate in 40 ms. If high concentrations of particles in aqueous suspension are delivered to macrophages, phagosomes will likely contain large particle clumps. The accretion process slows when chains of particles collapse into clumps and the magnetic moments of individual particles begin to cancel. Agglomeration can readily be observed in aqueous dispersions of magnetic particles, since sedimentation is seen to proceed far more quickly than expected for the primary particle size. Particle agglomeration is accentuated by the presence of strong external fields, such as may be used in particle magnetization. Each ferromagnetic particle will distort the field lines, producing strong local gradients which will augment particle–particle attraction due to the force $\mathbf{F} = (\mathbf{m} \cdot \nabla)\mathbf{B}$. In the case of airborne particles, the viscosity of air is 0.027 that of water, but particle concentrations are much lower. Even at an airborne concentration of $\rho_{\text{wt/vol}}$ = 0.2 mg/liter, the calculated agglomeration time is 1.4 h.

PARTICLE MOTION AND REMANENT MAGNETIC FIELD DECAY (RELAXATION)

Relation of the Remanent Field to Particle Orientation

The remanent field produced by particles of fixed magnetization will change if the particles are in motion. The net remanent magnetic field, measured in the z-direction, is given by the sum of individual moments, $\mathbf{m}_i$, from each of the N particles:

$$B_r(t) = \frac{\mu_0}{2\pi}\sum_{i=1}^{N}\frac{\mathbf{m}_i \cdot \hat{\delta}_z}{r_i^3}. \quad (25)$$

Since the distance between the particle-containing cells and magnetometer probes is fixed, the time dependence in this expression is contained in the dot product. The angular orientation of individual particles, $\theta_i(t)$, changes in time due to coupling with general cytoplasmic motion. If M_{tot} is the total moment of all magnetic particles and B_{r0} is the initial remanent magnetic field at t = 0 with moments aligned [$\theta_i(0) = 0°$], the remanent magnetic field can be written as

$$B_r(t) = B_{r0}\sum_{i=1}^{N}\frac{m_i}{M_{\text{tot}}}\cos[\theta_i(t)] = B_{r0}\langle\cos[\theta_i(t)]\rangle, \quad (26)$$

where the average is weighted by particle magnetic moments. Ideally, we would like to predict the $\theta_i(t)$'s (particle cytoplasmic motion) from the observations of $B_r(t)$ (magnetometric signals), but the inverse function for Eq. 26, $\theta_i(t) = F_i[B_r(t)]$, cannot be obtained. But if we postulate motions for the particles (the $\theta_i(t)$'s), then we can predict the time course of the remanent field [$B_r(t)$] and can compare the result to experimental data. The transfer function between "motility" and remanent magnetic field is controlled by how the particle angle distribution changes after magnetization. Immediately after magnetization all $\theta_i = 0°$. A long time after magnetization, the particle angles have become randomized with respect to the initial alignment along the z-axis.

As an example, we can predict the time course of the remanent field if the θ_i's are normally distributed about a mean, $\bar{\theta}$, with a variance σ^2 that increases linearly in time ($\sigma^2 = ct$). The angle distribution function is

$$f(\theta, t) = \frac{1}{\sqrt{2\pi ct}}\exp -\left[\frac{(\theta - \bar{\theta})^2}{2ct}\right], \quad (27)$$

and then

$$\langle\cos[\theta_i(t)]\rangle = \frac{1}{\sqrt{2\pi ct}}\int_{-\infty}^{+\infty}\exp -\left[\frac{(\theta - \bar{\theta})^2}{2ct}\right]\cos\theta\, d\theta \quad (28)$$

$$\langle\cos[\theta_i(t)]\rangle = e^{-ct/2}\cos\bar{\theta}. \quad (29)$$

For this example the remanent field would exhibit an exponential decay:

$$B_r(t) \propto e^{-ct/2}. \quad (30)$$

Examples of Mechanisms for Particle Motions

Remanent-field decay from particles within tissues and cells, relaxation, is due to rotation of particles away from the initial alignment direction. As the particles rotate, their magnetic field contributions tend to cancel, and the remanent field decreases. The following four examples are illustrations of mechanisms that may drive particle rotations: (*a*) twisting by magnetic fields, (*b*) elastic recoil, (*c*) random diffusive rotation, and (*d*) organelle pulling by linear tracks. These mechanisms can be expressed mathematically to facilitate comparison of predicted remanent-field decay curves with experimental data. The derivations necessarily involve some simplifying assumptions, which can be removed at the cost of more complexity and numerical rather than analytical solutions.

(*a*) Particle twisting by magnetic fields was derived earlier, and the result for remanent-field decrease as the

particles rotate away from the sensing direction was given in Eq. 11. Fig. 1 illustrated the time dependence for both the remanent field and the angular velocity for particles in a Newtonian fluid of 100 Pa-s viscosity. Twisting can be used to estimate intracellular hindrances to forced motion.

(*b*) Elastic recoil can drive particle reorientation. When particles are magnetized using a permanent magnet, they may be physically rotated away from their equilibrium angular location, θ_{eq}, to a final orientation, θ_{fn}. If the energy in this cytoplasmic rearrangement is elastically stored, then upon removal of the magnetizing field, the particle will recoil toward its equilibrium angle and produce a remanent-field decay. The rate of rotation (neglecting inertia) is determined by the balance between elastic torque $[\kappa V\nu(\theta - \theta_{eq})]$ and viscous retardation of rotation $(\kappa V\eta\dot{\theta})$:

$$\frac{\partial\theta}{\partial t} = -\frac{\nu}{\eta}(\theta - \theta_{eq}), \tag{31}$$

where ν is the rigidity modulus. If $\theta = \theta_{fn}$ at $t = 0$ at the end of magnetization, the solution for $\theta(t)$ is

$$\theta(t) = \theta_{eq}[1 - \exp(-\nu t/\eta) + \theta_{fn}[\exp(-\nu t/\eta)]. \tag{32}$$

If magnetization was applied along the z-axis ($\theta = 0$) and produced reorientation from θ_{eq} to θ_{fn}, then the remanent field decay measured along the z-axis due to elastic recoil can be obtained by substituting Eq. 32 into Eq. 26. The slope of the remanent-field decay at $t = 0$ is

$$\left(\frac{dB_r}{dt}\right)_{t=0} = -B_{r0}\frac{\nu}{\eta}(\theta_{eq} - \theta_{fn})\sin\theta_{fn}. \tag{33}$$

Interestingly, the contribution of elasticity to initial relaxation rate depends not only on the net angular twist produced by magnetization, but also on the final angle (θ_{fn}) between particle magnetization and applied magnetic field.

(*c*) Random diffusive (Brownian) rotation of particles was studied by Einstein (1956). He showed that in rotational Brownian motion the distribution function of particles angles, $f(\theta, \phi, t)$, obeys the diffusion equation,

$$\frac{\partial f(\theta, \phi, t)}{\partial t} = D\nabla^2 f(\theta, \phi, t),$$

$$\text{where} \quad \nabla^2 = \frac{1}{\sin\theta}\frac{\partial}{\partial\theta}\left(\sin\theta\frac{\partial}{\partial\theta}\right) + \frac{1}{\sin_2\theta}\frac{\partial^2}{\partial\phi^2}, \tag{34}$$

and where the coefficient of rotational diffusion, D, has units of $(s)^{-1}$ and is given by

$$D = \frac{kT}{\kappa V\eta} \quad \left(= \frac{kT}{\pi d^3\eta} \quad \text{for a sphere of diam} = d\right). \tag{35}$$

$f(\theta, \phi, t)$ represents the probability density as a function of azimuthal angle ϕ and polar angle θ relative to the z-axis. The diffusion equation describes a random walk over the surface of a unit sphere, and a general solution to this equation is

$$f(\theta, \phi, t) = \sum_{\substack{n=0 \\ -n\le m\le n}}^{\infty} A_{nm}e^{-n(n+1)Dt}Y_{nm}(\theta, \phi), \tag{36}$$

where the A_{nm} are arbitrary coefficients and the Y_{nm} are spherical harmonics. The measured remanent field for an assembly of particles is given by the sum of the components of particle magnetic moments that point along the measurement direction (z-axis). The net remanent field, $B_r(t)$, is given by the integral of ($f\cos\theta$) over all angular positions. Noting that $\cos\theta \propto Y_{10}$, and all other Y_{nm} are orthogonal, we have

$$B_r(t) = \frac{\int\cos\theta f(\theta, \phi, t)d^2\Omega}{\int f(\theta, \phi, t)d^2\Omega} = \frac{A_{10}e^{-2Dt}}{A_{00}}. \tag{37}$$

The aligned particle magnetic moments produce a net field of B_{r0} along $\theta = 0$ at $t = 0$, thus

$$B_r(t) = B_{r0}e^{-t/\tau_{dfsn}}, \quad \text{where} \quad \tau_{dfsn} = \frac{\kappa V\eta}{2kT}. \tag{38}$$

The decay of the remanent field due to random, diffusive motions is a simple exponential. If randomizing mechanisms are driven by other than thermal energies, kT in Eq. 38 can be replaced by a different source of energy, e.g., E_{cell} (Nemoto, 1982). Nevertheless, for any random-walk motions over the surface of a sphere, the time dependence of remanent-field decay is exponential.

In contrast to the case for particle rotation by magnetic fields, τ_{dfsn} is markedly dependent on particle size. Values for diffusion relaxation time (at 37°C) are shown in Table III for a range of diameters relevant to particles within cells. The smallest particle, 0.03-μm diam, is close to the lower size limit for stable magnetization. The relaxation time for typical particles (0.43-μm diam) within glycerol solutions (1 Pa-s viscosity) is nearly equivalent to times observed for particles within living cells. This illustrates the importance of determining intracellular viscosity when attempting to identify mechanisms of relaxation.

(*d*) Organelle pulling by linear tracks can be observed when particles within living cells are examined by videomicroscopy. Often, one end of an elongated particle-containing vesicle will remain anchored while the other end appears to be pulled to and fro in saltatory motion along a

TABLE III
DIFFUSIVE REORIENTATION TIME, τ_{dfsn}, AT 37°C

Equivalent sphere diam	Fluid viscosity η (Pa-s)		
	0.0007	1.0	1,200
μm			
11.0	5.7 min	5.7 d	18.7 yr
2.0	2 s	0.8 h	41 d
0.43	20 ms	29 s	9.7 h
0.03	7 μs	10 ms	12 s

"linear track," the result being random changes in angular orientation. This suggests a mathematical model where the angular direction of the magnetic moment vector is tethered to a linear track along which the attachment moves in a one-dimensional random walk, in contrast to the case just considered of random walk over the surface of a sphere. In this mechanism of particle magnetic moment reorientation, where the particle-containing vesicle is pulled primarily by one end, the particle angular position, θ, relative to an initially aligned position, $\theta = 0$, is given by

$$\tan\theta = \frac{s_\perp}{d}, \tag{39}$$

where $s_\perp$ is that component of net displacement along the track that is perpendicular to the original alignment direction, and d is the distance between the pivot and the movable attachment of the vesicle to the track. The motion of the track attachment is modeled as a one-dimensional random walk. If the step size is Δ, then after a large number, N, of steps, the probability of the displacement lying between x and $x + dx$ is given by the Gaussian

$$G(x)dx = \frac{1}{\sigma\sqrt{2\pi}} e^{-x^2/2\sigma^2} dx, \tag{40}$$

where $\sigma = \sqrt{N}\Delta$. The root mean-squared (rms) displacement is given by $\sqrt{\langle x^2\rangle} = \sqrt{\sigma^2}$, which increases as $\sqrt{N} \propto \sqrt{t}$ if the step size is constant. Since the cell and linear track have finite extent and also since the particle-containing vesicle cannot be stretched arbitrarily far, it would be more realistic to assume that step size decreases along the linear track as the net displacement moves farther from the starting point. Suppose the step size decreases as $x^{1-\beta}$, with $0 < \beta < 1$. The distribution of displacements can be evaluated using the transformation $y = x\{\Delta/x\}^{1-\beta}$, in which case

$$\begin{aligned}\langle y^2\rangle &= \int_{-\infty}^{+\infty} G(x) y^2 dx \\ &= \frac{\Delta^{2-2\beta}}{\sigma\sqrt{2\pi}} 2\int_0^\infty x^{2\beta} e^{-x^2/2\sigma^2} dx \\ &= \frac{\Delta^2}{\sqrt{\pi}} 2^\beta \left(\frac{\sigma}{\Delta}\right)^{2\beta} \Gamma(\beta + \tfrac{1}{2}).\end{aligned} \tag{41}$$

If the time per step is ϵ, the rms displacement along the x axis after a time $t = N\epsilon$ is

$$\langle y^2\rangle = \frac{\Delta^2}{\sqrt{\pi}} \Gamma(\beta + \tfrac{1}{2}) \left(\frac{2t}{\epsilon}\right)^\beta. \tag{42}$$

The angular orientation of the particle then changes as

$$\tan\theta = \frac{\sqrt{\langle y^2\rangle}}{d}. \tag{43}$$

The remanent field is given by

$$B_r(t) = B_{r0}\cos\theta = \frac{B_{r0}}{\sqrt{1 + \langle y^2\rangle/d^2}}. \tag{44}$$

This can be expressed as

$$B_r(t) = B_{r0}\left[1 + \left(\frac{\Delta}{d}\right)^2 \frac{\Gamma(\beta + \tfrac{1}{2})}{\sqrt{\pi}} \left(\frac{2t}{\epsilon}\right)^\beta\right]^{-1/2}. \tag{45}$$

For magnetic particles being moved about within living cells, β is found to be approximately one-half, in which case

$$B_r(t) = B_{r0}\left(1 + \sqrt{t/\tau_{cell}}\right)^{-1/2}, \tag{46}$$

where τ_{cell} is a time constant characteristic of cytoplasmic motion. This particular model is found to fit relaxation curves for isolated macrophages quite well. The average value of τ_{cell} for normal hamster lung macrophages after pulse magnetization is ~25 s.

In summary, the net angular motion of particles within cells may be composed of several mechanisms, including externally driven twisting, rotatory diffusion, elastic recoil, and internally driven reorientation by vesicle attachments. The theoretical expressions we have presented for remanent-field decay are examples that can be applied to modeling experimental relaxation curves. The goal is to describe both the intracellular forces driving relaxation and the apparent viscosity resisting these forces in fluid-mechanics terms.

PRODUCTION OF MAGNETIZING FIELDS

The intensity, duration, and spatial homogeneity of the magnetizing field are important determinants of the remanent field. The maximum remanent-field magnitude is achieved by magnetization to saturation, which requires ~125 mT in γ-Fe_2O_3. For moveable particles, such as intracellular ones, magnetization duration will determine if particles rotate to line up with the applied field or become magnetized in place, without cytoplasmic perturbation due to particle rotation. Generally, a uniform, parallel magnetizing field is desirable, otherwise the nonuniform magnetizing field acting on a nonuniform distribution of magnetic particles in an oddly shaped organ (e.g., lungs) can produce results that are both variable and difficult to interpret. However, Robinson (1981) has pointed out advantages of localized magnetization for purposes of increased sensitivity when imaging magnetic particle distributions. Magnetization can be accomplished using either permanent magnets or current-carrying coils. The important differences between these two methods are presented in the Appendix. In summary, permanent magnets are easily portable and require no power source. However, their use requires physical apposition of the magnet to the specimen; the fields produced are generally nonuniform and cannot be applied briefly. Electromagnets

can be made portable, can generate fields of predictable geometry over large volumes, and can be pulsed to allow particle magnetization in the absence of particle rotation. As will be reported in the subsequent paper (Valberg and Feldman, 1987), cytoplasmic relaxation measurements are affected by the duration of magnetization.

APPARATUS FOR CELL MAGNETOMETRY

Living cells maintained in oxygenated culture medium at 37°C will generally attach to glass or tissue culture plastic surfaces. The adherent, particle-containing cells are positioned in the apparatus shown in Fig. 5, where oxygenation is continued by a flow of air plus 5% CO_2 and temperature is maintained at 37°C by water flowing from a regulated bath. The particles in the cells are magnetized either within the apparatus by a pulse or outside the apparatus by a permanent magnet that is applied for seconds or minutes. Magnetic signals are sensed by four fluxgate magnetometer probes in a second-order gradiometer configuration (Fig. 6).

The remanent field produced at the end of magnetization is considerably weaker than environmental fields in a typical laboratory setting. The remanent field, B_r, is given by Eq. 25. For a mass w of material, magnetized in the z-direction, at a distance r from the sensor ($r >$ dimensions of the particle collection) the field is

$$B_r = \frac{\mu_o}{2\pi} \cdot \frac{\sigma_r w}{r^3}, \quad \text{where} \quad \sigma_r w = m. \tag{47}$$

σ_r is the remanent magnetization per kilogram (Table I). For example, 5 μg of γ-Fe_2O_3 produces a remanent field of ~0.17 nT at a distance of 5 cm. By contrast, the earth's magnetic field is 50,000 nT, and local sources of magnetic noise and 60 Hz interference are of order 10–100 nT. The

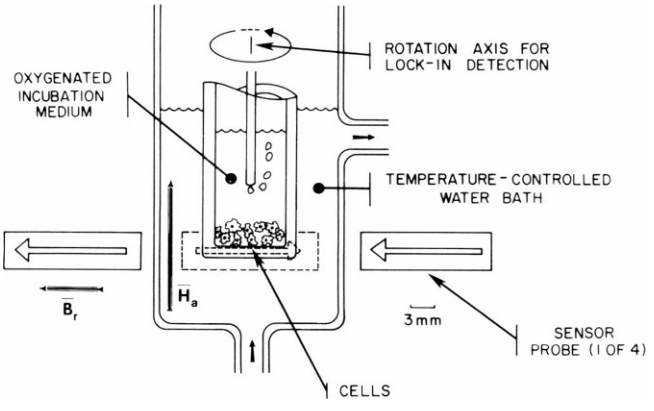

FIGURE 5 In vitro cell magnetometry apparatus used for measuring remanent field decay in cells containing magnetic particles. $\mathbf{B}_r$ displays the orientation of the remanent magnetic field relative to the leftmost fluxgate probe at the angular position, during vial rotation, of maximum sensitivity. $\mathbf{H}_a$ indicates the direction of the twisting magnetic field produced by a solenoid wound around the tube containing the temperature-controlled water.

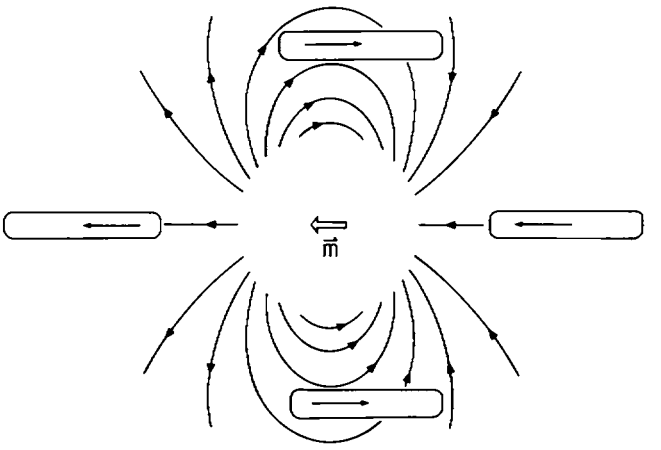

FIGURE 6 View of the magnetometry apparatus from above. The magnetic-particle containing cells are represented by a magnetic moment $\mathbf{m}$ that rotates about a vertical axis in the center of the probe array. This produces an alternating magnetic signal in the four probes whose sensitive axes are positioned as shown.

following noise-reduction and signal-enhancement measures are necessary to differentiate the field generated by particles within cells from environmental magnetic noise.

Magnetic Shielding

Magnetic shielding reduces the effect of large, slowly varying fields. Mu-metal and supermalloy are widely used as screening material because of their high initial permeability (10^4–10^5) and low coercivity (2–3 μT). For a cylinder of diameter D, wall thickness d, made from material having relative permeability μ, the shielding factor for transverse fields is given by (Freake and Thorp, 1971)

$$S = \mu(d/D). \tag{48}$$

For multiple coaxial cylinders, the resultant transverse shielding factor is

$$S_T = \Sigma S_i + \Pi S_i[1 - (A_i/A_{i+1})], \tag{49}$$

where A_i is the cross-sectional area of the ith cylinder. This formula indicates that using several, spaced cylinders is much more effective than a single, thick shield. Our apparatus uses three capped cylinders of supermalloy having diameters of 30.5, 35.5, and 40.5 cm and wall thicknesses of 0.65, 0.65, and 1.05 mm. For $\mu = 3 \times 10^4$, this gives a calculated shielding factor of 15,500. Such shielding can be realized for static magnetic fields by using a treatment called "degaussing," where coils driven by ac current magnetically saturate the shielding material in the presence of the static field. The ac current is slowly reduced to zero so that magnetic domains in the shields can accommodate to the local magnetic field (Cohen, 1971). The shielding factor is degraded by as much as 100-fold for slowly varying magnetic fields, where the limitation is the

nonzero coercivity of the material. For rapidly time-varying magnetic fields, shielding increases again due to eddy currents induced in the shields. In fact, the skin depth (the penetration for 1/e attenuation) is 0.37 mm for 60 Hz fields in mu-metal, and penetration decreases with increasing frequency (as $1/\sqrt{f}$).

Probe Positioning

Probe positioning can be adjusted so that the sensitivity to the local remanent field is enhanced while the effects of more distant sources are canceled (Williamson and Kaufman, 1981). The four fluxgate detectors are oriented parallel to the magnetic dipole field lines from the nearby particle-containing cells in what is known as a second-order gradient configuration (Fig. 6). The remanent field magnitude along the axis of the dipole is given by Eq. 47. B_r perpendicular to the dipole axis is oppositely directed (and one-half the magnitude at the same r). When the signals from the probes are summed, the contributions from the cell vial dipole add to give a net signal ~3× that from a single fluxgate probe. The contributions from uniform or uniform-gradient fields cancel.

Lock-in Amplification (Phase-sensitive Detection)

Lock-in amplification is a final measure, which not only aids in rejection of noise from environmental sources but which also eliminates contributions from baseline drift in the magnetometer or temperature drift in the fluxgate detector probes. The vial with its adherent cells is rotated at ~13 Hz in the center of the fluxgate array, and only those magnetic signals in synchrony with the rotation rate are selectively detected and amplified (model 393 lock-in amplifier; Ithaco, Inc., Ithaca, NY). This effectively eliminates drift, $1/f$ background noise, and 60-Hz interference. The time constant of the cell magnetometer is ~0.2 s and is influenced both by vial rotation rate and lock-in amplifier averaging time. The rotating vial carrier is air-driven and constructed of nonmetallic materials to avoid generation of spurious magnetic signals. Vial carriers are interchangeable and slide into position from above, so that different cell samples can be presented in quick succession.

In whole-animal studies, separation of signal from noise is achieved by moving the animal in proximity to and then away from the fluxgate probes (Cohen, 1975; Gehr et al., 1983*a*, *b*; Brain et al., 1984). Such "near-far" motions are similar to phase-sensitive detection in that they compensate for baseline drift. The relaxation curve must be interpolated between readings and observation of rapid transients is difficult. Furthermore, if the animal and probes are in close apposition at the "near" position, the signals become exquisitely sensitive to changes in the exact location and orientation of "near," due to the $1/r^3$ dependence and vector nature of the remanent field. In the cell apparatus described here, the relative distances between probes and cell vial are held constant, assuring that changes in magnetic field do not arise from distance or orientation variability.

Whereas in vivo studies have required ~200 μg of iron oxide for magnetic detection, the above arrangement in combination with a fluxgate bar-core magnetometer (model 1.104 oerstedmeter; Förster, Reutlingen, FRG) can record relaxation curves for quantities as small as 2 μg ($S/N > 10$). The sensitivity and noise level of a ring-core fluxgate magnetometer (model RCS-01 quad magnetometer; Nanotesla, Inc., Silver Spring, MD) allows accurate measurement of remanent-field decay from ~0.2 μg of magnetic iron oxide ($S/N > 10$). Fig. 7 illustrates the signal-to-noise levels for the fluxgate cell magnetometer when detecting the remanent magnetic field from 0.8 μg of randomly oriented γ-Fe_2O_3 particles previously magnetized to saturation. A SQUID (superconducting quantum interference device) magnetometer could provide even more sensitivity, but currently requires cryogenic temperatures for the operation of its sensor elements (Williamson and Kaufman, 1981).

For determination of the apparent viscosity of the particle environment, the response of magnetized particles to a magnetically driven reorientation (a "twist") is measured. A field perpendicular to the particle magnetization direction is generated by a two-layer solenoid wound with its axis along the axis of vial rotation (1.8-cm diam, 5.6-cm long, 250 turns). The magnetic field produced (~2.5 mT at 0.5 A current) applies a torque to the horizontal magnetic dipoles acting to twist them into a vertical orientation and out of the plane of sensitivity of the magnetometer probes. The magnetometer probes, both by virtue of their directional sensitivity (Figs. 5 and 6) and as a result of the phase-sensitive detection, do not respond to this static field, but the fall in remanent magnetic field resulting from

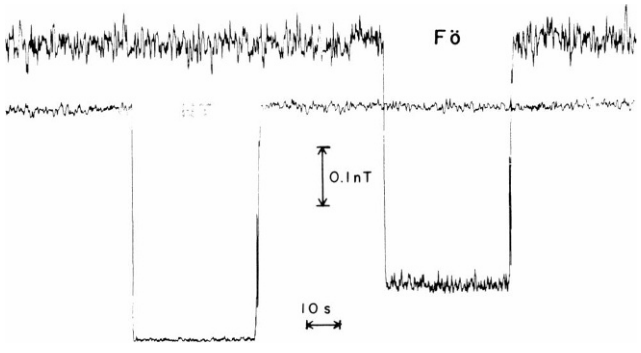

FIGURE 7 Chart recorder output of the overall magnetometry detection system (magnetic shields, gradiometric probe configuration, and lock-in amplification) showing the signal response to 0.8 μg of γ-Fe_2O_3. The S/N ratio for the Förster 1.104 magnetometer (*Fö*) is ~5 and S/N for the Nanotesla RCS-01 magnetometer (*NT*) is ~40. The noise bandwidth shown here has been narrowed to 1.3 Hz at a center frequency of 13 Hz for both magnetometers. The full-scale response time demonstrated for a step change (presence or absence of the γ-Fe_2O_3) is ~1.8 s. The vertical displacement of the two tracings has been introduced for clarity.

particle twisting can be followed magnetometrically. The rate of particle reorientation is related to apparent viscosity as given by Eq. 11. Experimental results on cytoplasmic motility and on apparent cytoplasmic viscosity are presented in the following paper (Valberg and Feldman, 1987).

The calibration of the magnetometer system in terms of quantity of γ-Fe_2O_3 can be accomplished by magnetizing known weights of material collected from the aerosol on sampling filters. Absolute calibration in terms of magnetic moment can be obtained using a coil of known dimensions carrying a known current, since the magnetic dipole moment of a current, i, flowing in a loop of area S is $m = iS$.

DISCUSSION

We have presented the physical principles involved in the use of magnetic particles to probe cytoplasmic mobility. The interpretation of experimental results requires understanding the behavior of magnetic particles in fluids. Models for remanent-field decay were proposed and time constants calculated. Theoretical aspects of human magnetometry have been discussed elsewhere (Nemoto, 1982; Cohen and Nemoto, 1984; Cohen et al., 1984), and we have not attempted an exhaustive coverage of all areas in our analysis. The goal has been to show how both magnetometric observation and twisting of magnetic particle–containing organelles can provide parameters by which to express both spontaneous motion in living cells and cytoplasmic resistance to driven rotation. Further theoretical or numerical calculations will be needed as more experimental data become available. Some important points regarding simplifications and interpretations pertinent to our analysis merit discussion.

Particle Geometry and Remanent-Field Magnitude

Magnetic particles found in cells and tissues are generally not uniform in size or shape, and the effects on relaxation of various particle size and shape distributions are difficult to evaluate. Intracellular particles can also change their geometry by dissolution or agglomeration. If size and shape distributions are known, the analysis can be applied to each fraction in turn to derive a result for the complete distribution. Rotation in magnetic fields is relatively insensitive to particle size (Eq. 11), but diffusive rotation (Eq. 38) is markedly dependent on size. Also, particle remanent magnetization (moment per unit mass) falls with increasing size if there is volume taken up by domain walls (Stacey, 1962).

Particle Motions

Particle motions may be affected by interparticle magnetic interactions. We have only considered actions of one dipole on another (Eqs. 17 and 24). A more complete treatment would include interactions among all particles. The distribution of particles in space is an important factor. If a sheet of particles is magnetized perpendicular to that sheet (such as particles in the bottom of a petri dish), then particles will act to rotate each other into antiparallel alignment and relaxation rate will be enhanced. If an elongated distribution of particles is magnetized parallel to the long axis (such as is found in magnetotactic bacteria), particles interact with each other to stabilize their orientation and inhibit relaxation. For a spherical distribution of magnetic dipoles there is no net effect.

Viscosity Measurements

The cytoplasm is likely non-Newtonian, with many filamentous elements that may be linked to the phagosomes containing the magnetic particles. Identification of the locale at which fluid shear takes place in intact cells is difficult, and assignment of an absolute viscosity value impossible. A considerable body of knowledge exists treating the rheology of complex polymer networks (Doi and Edwards, 1986), but we did not attempt to include non-Newtonian viscosity. Nonetheless, magnetometric measurements of intact cells can yield useful results for "apparent mobility" and "apparent viscosity." All approaches to studying cytoplasmic motions or viscosity require cautious interpretation. Only cone-and-plate rheometers produce uniform shear. For example, the pulling of particles within cells or purified protein gels produces nonuniform shear and can only yield an apparent viscosity. However, some important differences between twisting and pulling measurements of apparent viscosity make twisting preferable.

(a) The effect of particle size variation on apparent viscosity determination is less acute in twisting as compared with pulling. In twisting, the magnetic torque is proportional to particle mass or a^3 (a = radius); the viscous drag retarding rotation is also proportional to a^3 (Eqs. 2 and 4). Thus, the rotation rate (ω) of the particle is to first-order independent of particle size. The fluid shear rate, which is proportional to the rotation rate, is also independent of particle size. This is in contrast to linear motion, where viscous force is proportional to particle size ($6\pi\eta a v$), and magnetic force is proportional to particle volume (a^3), which means particle velocity is proportional to a^2. Since velocity is the observed quantity, results for viscosity are very sensitive to particle size. In linear motion, the shear rate is given by the time needed for the particle to transverse its own length, $t = a/v$, which would be proportional to a^{-1}. Therefore, in pulling it is crucial to know the particle radius accurately, whereas in twisting, the results are independent of size per se.

(b) Particle shape effects on twisting and pulling in a viscous fluid can be calculated for the idealized case of ellipsoids having major axis a and minor axis b (Flügge, 1963). For pulling with constant force, as (a/b) goes from

1 to 5, there is a threefold change in particle velocity. However, for twisting with constant torque, as (a/b) goes from 1 to 5, the rate of particle rotation changes <10%. Exact solutions cannot be obtained for particles of arbitrary shape, but again, the situation is less troublesome in twisting than in pulling.

(*c*) Boundary effects are more significant in pulling than twisting. This derives from the fact that the fluid velocity at a distance, r, from a pulled sphere falls off as (a/r), whereas fluid velocity falls off much more rapidly, as $(a/r)^3$, from a rotating sphere (Lamb, 1932). The correction factor to viscous torque on a sphere of radius a twisted within a fixed sphere of radius R, as compared with a sphere twisted in an infinite sea of material, is $[1 - (a^3/R^3)]^{-1}$ (Lamb, 1932). For a sphere of radius 1 within a larger one of radius 2, the correction factor if only 1.1. However, Ladenburg's and Faxen's (Faxen, 1922) correction to the viscous force on a pulled sphere under the same conditions would be a factor of ~5.6. Hence, boundaries are less likely to dominate viscosity results in the case of twisting. Also, translocation through the cytoplasm may be more disruptive of cell structures than rotation in place.

Negative Clearance

Once particle influx stops, the amount of material in the lungs decreases with time due to clearance mechanisms. Yet increases in remanent magnetic field over the chest of an animal or human for as long as a week after a magnetic particle inhalation exposure have been reported (Cohen and Nemoto, 1984; Freedman et al., 1985). The cause of negative clearance artifacts is unclear, but possible mechanisms include (*a*) redistribution, (*b*) particle mobility change, (*c*) clumping, and (*d*) breakup of clumps.

(*a*) Redistribution refers to the fact that remanent field measurements are sensitive to the position of magnetic material. This derives both from the vector nature of the magnetic field and the fact that the magnitude of a particle's contribution drops as the cube of the distance. Hence, movement of material from the lung periphery towards the hilum (central regions) may cause the remanent field measured at the hilum to increase. In addition, Robinson has shown that the remanent field can be highly sensitive to lung configuration, even with particles distributed uniformly (1981).

(*b*) Particle mobility change could cause the effect in two ways. At early times after inhalation exposure, particles may be in an aqueous environment, and Brownian rotation may be so rapid that some particles are "invisible" to a remanent field measurement which takes several seconds. The remanent field will decrease by $1/e$ in a time, τ_{dfsn} (Table III), which for a ½-μm particle in water is 20 ms. Over several days, such particles may become constrained in lung tissues become detectable. Conversely, if elongated single-domain particles are trapped in a highly viscous environment, particles with their long axis perpendicular to the magnetization direction will not contribute to remanent field because of self-demagnetization (Eq. 1). As a consequence of the repeated magnetizations used in following clearance magnetometrically, these particles may slowly become aligned with the applied field direction and begin to contribute to remanent field. This mechanism was suggested by Cohen and Nemoto (1984) to explain remanent field increases observed in humans over the first day after magnetic-particle inhalation.

(*c*) Clumping refers to the fact that a certain fraction of the inhaled particles may be small enough to be superparamagnetic. Again, these particles, which would initially be magnetometrically "invisible," can become agglomerated by phagocytosis or by successive magnetizations, and then contribute to the remanent field.

(*d*) Breakup of clumps can also result in increased remanent field if the close proximity of initially deposited particles causes them to act on one another after magnetization to physically rotate into antiparallel alignment. If, over a period of time, the particles become dispersed, they will then no longer magnetically interact to produce such cancellation. Breakup of particle clumps due to macrophage ingestion was a factor suggested Cohen and Nemoto (1984) to explain remanent field increases. Microscopy of lung tissues, however, suggests that macrophages act to collect together widely dispersed particles rather than disaggregate them (Sorokin and Brain, 1975).

Summary

Magnetic fields from intracellular magnetic particles can be used to investigate macrophage motile function without the need for optical observation by microscope. When evaluating the magnetometric results obtained in living systems, one needs to consider carefully both the response of the magnetometric measurement apparatus and the magnetic behavior of small particles. Known forces can be applied to intracellular particles using external magnetic fields, and the resistance to motion can be assessed. This may allow measurement of changes in cytoplasmic consistency accompanying cell functions such as endocytosis, exocytosis, intracellular transport, activation, shape change, and translocation.

APPENDIX

Magnetization Methods

Permanent magnets have the advantage of simplicity, portability, and no requirement for power. Important considerations in their use include (*a*) calibration of the field magnitude and direction as a function of distance from the pole face, (*b*) applying and removing the magnet so field lines are always parallel to the magnetization desired in the specimen, and (*c*) being certain that no particles of material from the magnet contaminate the specimen. Cohen (1978) successfully used a 5 × 5-cm pole face × 20-cm-long Alnico bar magnet for magnetization of human subjects.

Small cobalt-samarium magnets, 2.5 × 2.5 cm with a 1-cm pole separation producing 300 mT at the magnet face, have been used for small-animal magnetization (Gehr et al., 1983*a*, *b*). But the field drops off rapidly, being only 80 mT at 1 cm from the magnet, a level at which the remanent field is sensitive to small variations in the magnetizing field. At 2.2 cm the field has dropped to 25 mT, which is below the coercivity of magnetic iron oxides; magnetization can now occur only by physical rotation of particles having a nonzero magnetic moment. Samples of isolated cells are small and can be magnetized by a field generated by two 2.5-cm diam Co-Sm permanent magnets enclosed in a soft-iron yoke that assures uniform field (210 mT) over the cell vial.

Solenoids and Helmholtz coils have the advantages that (*a*) the fields produced can be calculated (Eqs. A1 and A2), (*b*) homogeneity in the field can be achieved over a considerable volume, (*c*) physical movement of the specimen in the process of magnetization is not required since the field can be turned on and off, and (*d*) contamination with magnetic material cannot occur. Helmholtz coils have been used by Kalliomäki and colleagues (1976). Cohen (1978) used aluminum "pancake" coils in a Helmholtz configuration generating 100 mT and powered by either car batteries or dc current from a welding supply.

Pulsed coils can be used to magnetize particles quickly, while actually within the magnetometer. Since movement of magnetic domain boundaries in nonconducting particles is rapid (~35 μm/μs), small particle magnetization is complete in <1 μs. In such a short period of time, no particle rotation can take place (see Table II). A large current pulse can be generated by discharging a capacitor into a coil. Resistive heating is minimal because of the short duration of the pulse. As shown below, the controlling factors are the inductance of the coil and the size of the capacitor, with R adjusted for critical damping. Table IA illustrates the interactions of the design parameters for Helmholtz coils. It can be seen that high field, short time constant, and large magnetized volume are difficult to achieve simultaneously. The time course of the magnetic field pulse generated by critically damped 12-turn, 3-cm-diam Helmholtz coils is shown in Fig. 1, *top*. Critical damping need not be exactly achieved as long as the reverse current in the underdamped case is small (or is shorted via a diode), or as long as the somewhat longer pulse duration in the overdamped case is not of concern.

The axial magnetic field of a solenoid of n turns/meter with current i is

$$H_a = ni[\tfrac{1}{2}(\cos\theta_1 + \cos\theta_2)], \tag{A1}$$

where θ_1 and θ_2 are the angles between the solenoid axis and the outer edges of the solenoid ends as seen from the measurement point. Helmholtz coils, with N turns each, having a radius and separation, a, generate a field

$$H_a = \frac{1.6Ni}{\sqrt{5}\,a}. \tag{A2}$$

TABLE IA
HELMHOLTZ PULSE COIL CHARACTERISTICS

Parameter	Cells		Animals	
Coil diameter, $2a$	3 cm		40 cm	
Peak field, H_a	145 mT		145 mT	
Pulse peak, τ	1.2 μs		100 μs	
N, turns per coil	1	12	1	6
V_0, volts	750	9,000	1,500	9,000
L, μH	0.13	19.0	1.8	64.0
C, μF	12.0	0.08	5,600	156
R, Ω	0.22	32.0	0.036	1.3

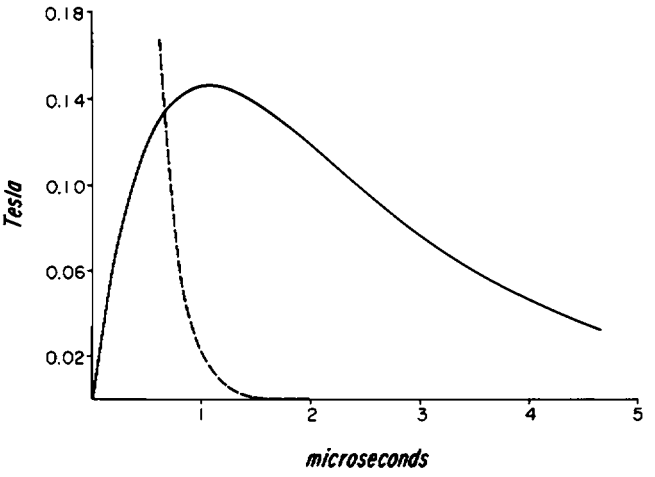

FIGURE 1A Time course of the pulsed magnetic field for the coil and capacitor configuration used for in vitro macrophage experiments ("Cells" in Table IA). The solid line refers to the magnetic field and time scales as given; the dashed line shows the tail of the pulse, with the values on the x-axis now being tens of microseconds, and the y-axis magnetic field now being one-tenth of the values shown.

For a critically damped L, R, C circuit in which a capacitor initially charged to V_0 is connected to L and R in series, the current is given by

$$i = \frac{2V_0}{R}\frac{t}{\tau}\exp(-t/\tau), \tag{A3}$$

with τ defined as

$$\tau = 2L/R \quad \text{and} \quad C = 4L/R^2 \quad \text{for critical damping} \tag{A4}$$

and

$$L = k\mu_0 N^2 a \qquad \text{for Helmholtz coils.} \tag{5}$$

(k is a geometrical constant; for Helmholtz coils k = 6.9 [Terman, 1943]). The peak current occurs at $t = \tau$. For Helmholtz coils of radius a, N turns each, the energy stored in the capacitor is related to the peak magnetic field:

$$\tfrac{1}{2}CV_0^2 \approx 50\mu_0 H_a^2 a^3. \tag{A6}$$

The requirements for voltage and capacitance increase dramatically with coil area. The capacitance, C, is limited in size by the criterion for critical damping, which relates it to the desired time constant, τ:

$$C_{crit} = \frac{(\tau/N)^2}{\mu_0 ka} \quad \text{and } R \text{ is then given by} \quad R = 2\tau/C_{crit}. \tag{A7}$$

It is useful to know the time course of the current if critical damping is not exactly achieved. In the underdamped case

$$i = \frac{2V_0}{R}\exp(-t/\tau)\frac{\sin(D_u t/\tau)}{D_u}$$

$$t_{peak} = \tau\left[\frac{\tan^{-1}(D_u)}{D_u} + \frac{n\pi}{D_u}\right] \qquad \text{where } n = 0, 1, \ldots \tag{A8}$$

where

$$D_u = \sqrt{4L/R^2C - 1}.$$

And in the overdamped case

$$i = \frac{2V_o}{R} \exp(-t/\tau) \frac{\sin(D_o t/\tau)}{D_o}$$

$$t_{peak} = \tau \frac{\tanh^{-1}(D_o)}{D_o} \tag{A9}$$

where

$$D_o = \sqrt{1 - 4L/R^2C}.$$

The authors thank S. B. Bloom, J. D. Brain, D. Cohen, H. A. Feldman, and E. M. Purcell for help and advice.

This work was supported by National Institutes of Health grants CA-40696, ES-00002, and HL-31029.

Received for publication 2 February 1987 and in final form 4 May 1987.

REFERENCES

Bate, G. 1980. Recording materials. *In* Ferromagnetic Materials. E. P. Wohlfarth, editor. Elsevier North-Holland, New York. 381–507.

Brain, J. D., S. B. Bloom, P. A. Valberg, and P. Gehr. 1984. Correlation between the behavior of magnetic iron oxide particles in the lungs of rabbits and phagocytosis. *Exp. Lung Res.* 6:115–131.

Brown, W. F. 1962. Magnetostatic Principles in Ferromagnetism. Elsevier North-Holland, Amsterdam. 279 pp.

Cohen, D. 1971. Large-volume conventional magnetic shields. *Rev. Phys. Appl.* 5:53–58.

Cohen, D. 1973. Ferromagnetic contaminants in the lungs and other organs of the body. *Science (Wash. DC).* 180:745–748.

Cohen, D. 1975. Measurements of the magnetic fields produced by the human heart, brain, and lungs. *IEEE (Inst. Electr. Electron. Eng.) Trans. Mag.* MAG-11:694–700.

Cohen, D. 1978. Report of the Low-Field Group: The Magnetic Field of the Lung. Publication MIT/FBNML-78/1. Nat. Tech. Inform. Service, Springfield, VA.

Cohen, D., and I. Nemoto. 1984. Ferrimagnetic particles in the lung. Part I: The magnetizing process. *IEEE (Inst. Electr. Electron. Eng.) Trans. Biomed. Eng.* BME-31:261–273.

Cohen, D., I. Nemoto, L. Kaufman, and S. Arai. 1984. Ferrimagnetic particles in the lung. Part II: The relaxation process. *IEEE (Inst. Electr. Electron. Eng.) Trans. Biomed. Eng.* BME-31:274–285.

Doi, M., and S. F. Edwards. 1986. The Theory of Polymer Dynamics. Clarendon Press, Oxford. 391 pp.

Edwardes, D. 1893. Steady motion of a viscous liquid in which an ellipsoid is constrained to rotate about a principal axis. *Q. J. Pure Appl. Math.* 26:70–78.

Einstein, A. 1956. Investigations on the Theory of Brownian Movement. Dover, Mineola, NY. 119 pp.

Faxen, H. 1922. Die Bewegung einer starren Kugel langs der Achse einer mit zaher Flussigkeit gefullten Rohres. *Arkiv. Mat. Astron. Fyzik.* 17:1–28.

Flügge, S. 1963. Handbuch der Physik: Band VIII, Strömungsmechanik II. Springer-Verlag, Berlin. 352 pp.

Freake, S. M., and T. L. Thorp. 1971. Shielding of low magnetic fields with multiple cylindrical shells. *Rev. Sci. Instrum.* 42:1411–1413.

Freedman, A. P., S. E. Robinson, and R. J. Johnston. 1980. Non-invasive magnetopneumographic estimation of lung dust loads and distribution in bituminous coal workers. *J. Occup. Med.* 22:613–618.

Freedman, A. P., S. E. Robinson, and M. R. Street. 1985. Using magnetopneumography for studying the influence of cigarette smoking and lung disease on alveolar clearance in man. *In* Biomagnetism: Applications and Theory. H. Weinberg, G. Stroink, and T. Katila, editors. Pergamon Press, New York. 422–425.

Gehr, P., J. D. Brain, S. B. Bloom, and P. A. Valberg. 1983*a*. Magnetic particles in the liver: a probe for intracellular movement. *Nature (Lond.).* 302:336–338.

Gehr, P., J. D. Brain, I. Nemoto, and S. B. Bloom. 1983*b*. Behavior of magnetic particles in hamster lungs: estimates of clearance and cytoplasmic motility. *J. Appl. Physiol. Respir. Environ. Exercise Physiol.* 55:1196–1202.

Kalliomäki, P.-L., P. J. Karp, T. Katila, P. Mäkipää, P. Saar, and A. Tossavainen. 1976. Magnetic measurements of pulmonary contamination. *Scand. J. Work Environ. Health.* 4:232–239.

Kalliomäki, K., P. L. Kalliomäki, V. Kelhä, and V. Vaaranen. 1980. Instrumentation for measuring the magnetic lung contamination of steel welders. *Ann. Occup. Hyg.* 23:175–184.

Lamb, H. 1932. Hydrodynamics. Dover, Mineola, NY. 738 pp.

Nemoto, I. 1982. A model of magnetization and relaxation of ferrimagnetic particles in the lung. *IEEE (Inst. Electr. Electron. Eng.) Trans. Biomed. Eng.* BME-29:745–752.

Nemoto, I., H. Toyotama, P. Gehr, and J. D. Brain. 1985. *In vivo* and *in vitro* measurements of magnetic relaxation in hamster pulmonary macrophages. *In* Biomagnetism: Applications and Theory. H. Weinberg, G. Stroink, and T. Katila, editors. Pergamon Press, New York. 433–437.

Robinson, S.E. 1981. Magnetopneumography: non-invasive imaging of magnetic particulate in the lung and other organs. *IEEE (Inst. Electr. Electron. Eng.) Trans. Nucl. Sci.* NS-28:272–274.

Sorokin, S. P., and J. D. Brain. 1975. Pathways of clearance in mouse lungs exposed to iron oxide aerosols. *Anat. Rec.* 181:581–626.

Stacey, F. D. 1962. A generalized theory of thermoremanence, covering the transition from single-domain to multi-domain magnetic grains. *Philos. Mag.* 7:1887–1900.

Terman, F. E. 1943. Radio Engineers' Handbook. McGraw-Hill Book Co., New York. 1019 pp.

Valberg, P. A. 1984. Magnetometry of ingested particles in pulmonary macrophages. *Science (Wash. DC).* 224:513–516.

Valberg, P. A., and D. F. Albertini. 1985. Cytoplasmic motions, rheology, and structure probed by a novel magnetic particle method. *J. Cell Biol.* 101:130–140.

Valberg, P. A., and H. A. Feldman. 1987. Magnetic particle motions within living cells: measurement of cytoplasmic viscosity and motile activity. *Biophys. J.* 52:000–000.

Williamson, S. J., and L. Kaufman. 1981. Biomagnetism. *J. Mag. Mag. Materials.* 122:129–202.